Materials Letters 324 (2022) 132676

Contents lists available at ScienceDirect

Materials Letters

journal homepage: www.elsevier.com/locate/matlet

Novel as-cast NiAlCoFeNb dual-phase high-entropy alloys with high hardness

Lei Gu [1], Ningning Liang [1], Yi Liu, Yuyao Chen, Jihua Liu, Yixing Sun, Yonghao Zhao [*]

Nano and Heterogeneous Materials Center, School of Materials Science and Engineering, Nanjing University of Science and Technology, Jiangsu 210094, China

ARTICLE INFO

Keywords:
Metals and alloys
Microstructure
Crystal structure
Microhardness
B2 phase
Laves phase

ABSTRACT

The microstructure, phase constitution and microhardness of $Ni_{20}Al_{20}Co_{20}Fe_{20}Nb_{20}$, $Ni_{25}Al_{25}Co_{20}Fe_{20}Nb_{10}$ and $Ni_{30}Al_{30}Co_{20}Fe_{15}Nb_5$ high-entropy alloys (HEAs) synthesized by vacuum arc melting have been investigated. These as-cast HEAs have a dual-phase structure including intermetallic NiAl-rich B2 phase and FeNb-rich hexagonal Laves phase, and the Nb increase leads to more fraction of Laves phase. Ultrahigh hardness of ~ 818 HV was achieved in the equiatomic $Ni_{20}Al_{20}Co_{20}Fe_{20}Nb_{20}$ dual-phase HEA, which is consisted of 61.8 vol% Laves phase and 38.2 vol% B2 phase.

1. Introduction

As a fire-new alloy design concept, high-entropy alloys (HEAs) have been widely investigated since invented by Ye et al., [1] and Cantor et al., [2] in 2004. HEAs are comprised of multiple principal elements with equiatomic or near equiatomic composition, differing from conventional alloys based on one or two dominant elements [3,4]. Single-phase face-centered cubic (FCC) HEAs generally have high plasticity and ductility but low strength and hardness. Severe plastic deformation (SPD) has been employed to improve the strength and hardness by introducing high-density lattice defects [5,6]. For instance, the hardness of an equiatomic FCC CoCrFeMnNi HEA increased significantly from the initial ~ 160 HV to ~ 520 HV after high-pressure torsion treatment [7]. Although SPD processing can enhance the hardness of single-phase FCC HEAs, the maximum hardness is not high enough for industrial applications.

Apart from work hardening, introducing the second phase can effectively improve the hardness. In fact, the selection of alloying elements plays a crucial role on phase formation, and then significantly influences the properties of HEAs. As a prominent strengthening element, Al was generally added in FCC HEAs, which can facilitate the formation of body-centered cubic (BCC) or ordered B2 phases. With increasing the concentration of Al element in single-phase FCC CoCrFeNi alloy, the volume fraction of BCC phase increased, leading to the enhanced hardness [8]. Nb is also a significant substitutional element which can strengthen CoCrFeNi alloy. With the increase of Nb content, a hard Laves phase was formed and the volume fraction gradually increased in a series of $CoCrFeNiNb_x$ HEAs, contributing to an enhancive strength and hardness [9]. Laves phase reinforced alloys generally exhibit high thermal stability and excellent high temperature mechanical properties [10].

Therefore, in present work, Al and Nb were selected to add into CoFeNi alloy in order to synthesize a novel class of NiAlCoFeNb HEAs with ultrahigh hardness. The microstructure and phase constitution of these HEAs were investigated in details.

2. Experimental materials and procedures

Three HEAs ingots containing $Ni_{20}Al_{20}Co_{20}Fe_{20}Nb_{20}$, $Ni_{25}Al_{25}Co_{20}Fe_{20}Nb_{10}$ and $Ni_{30}Al_{30}Co_{20}Fe_{15}Nb_5$ (at%) were prepared by arc-melting a mixture of commercial metals (Purity > 99.9%) and labeled as Nb20, Nb10 and Nb5 based on Nb content. Phase structure was characterized by x-ray diffraction (XRD) with the angle of 2θ scanning from 20° to 90°. Microstructure and element distribution were investigated by scanning electron microscopy (SEM) equipped with energy dispersive spectroscopy (EDS) and electron backscatter diffraction (EBSD) detectors. The specimen for transmission electron microscopy (TEM) observation was prepared by ion milling and then observed at 200 kV. Vickers microhardness tests were conducted with a load of 4.9 N for 15 s and at least ten randomly indentations were tested to obtain a mean value.

* Corresponding author.
E-mail address: yhzhao@njust.edu.cn (Y. Zhao).
[1] Authors contributed equally.

https://doi.org/10.1016/j.matlet.2022.132676
Received 28 March 2022; Received in revised form 4 May 2022; Accepted 15 June 2022
Available online 17 June 2022

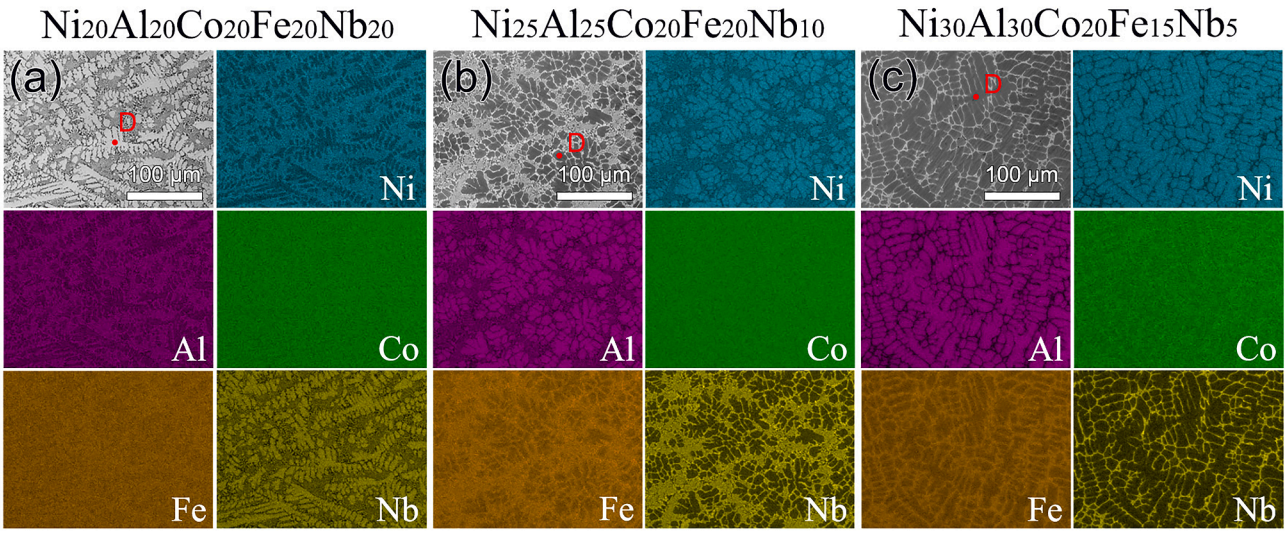

Fig. 1. SEM images and corresponding EDS mappings of (a) Nb20, (b) Nb10 and (c) Nb5 HEAs. The regions of dendrites are marked as D.

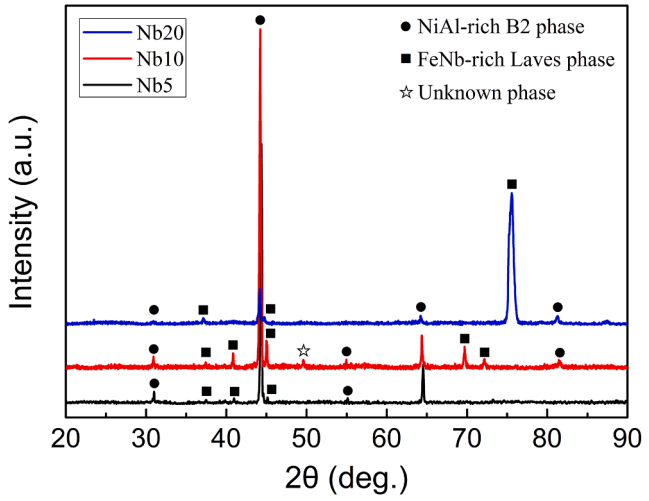

Fig. 2. XRD patterns of Nb20, Nb10 and Nb5 HEAs.

3. Results and discussion

The microstructure and element distribution maps of all three as-cast HEAs are shown in Fig. 1. There are two different regions in all samples, including dark-gray and light-gray regions. The distributions of chemical compositions from EDS mappings indicate that Ni and Al mainly aggregate in the dark-gray regions, while Fe and Nb prefer to exist in the light-gray regions. Specially, Co element almost uniformly distributes over the whole regions in Nb20 and Nb10 alloys, but slightly enriched in the light-gray regions of Nb5 alloy. It indicates that Co has very high solid solubility and plays effective role in solution strengthening in both phases. It can be found the volume fraction of the FeNb-rich regions increased as the concentration of Nb increased. Eventually, the dendritic regions (D regions in Fig. 1) evolved from the NiAl-rich regions of Nb5 and Nb10 alloys to the FeNb-rich regions of Nb20 alloy.

The crystal structures of the NiAl-rich phase and FeNb-rich phase were further identified by XRD, as shown in Fig. 2. In accord with the EDS result, Nb5 alloy is mainly composed of the NiAl-rich B2 phase and the remaining diffraction peaks correspond to the FeNb-rich phase. According to the Fe-Nb equilibrium phase diagram, there are two stable intermetallic compounds including the Fe_2Nb phase with a topologically close-packed (TCP) hexagonal structure (i.e. Laves phase) and the Fe_7Nb_6 phase with a TCP rhombohedral structure (i.e. μ phase) [11]. Although the atomic ratio of Fe/Nb is nearly 7:6 in the FeNb-rich phase of Nb5 alloy, the FeNb-rich phase is a hexagonal Laves phase (space group P63/mmc) from XRD analysis. This may be caused by the substitutional elements in the multi-component intermetallic compounds. Comparatively, more new diffraction peaks corresponding to Laves phase and a small number of unknown phase were produced in Nb10 alloy and all intensity also increased. For Nb20 alloy, the relative intensity of Laves phase is higher than that of B2 phase, revealing that the main phase transformed into Laves phase. Furthermore, it is noteworthy that the (1 1 0) diffraction peak of B2 phase gradually shifts towards smaller 2θ value with increasing Nb content, implying an incremental lattice constant of B2 phase. The increscent lattice constant is caused by the enhanced solid solubility of Nb element from 1.4 at% to 4.0 at% in the multi-component B2 phase.

The microstructures of three HEAs were further characterized by EBSD, as shown in Fig. 3. Nb20 alloy comprises a high volume fraction of dendritic FeNb-rich phase and a small amount of eutectic NiAl-rich phase/FeNb-rich phase lamellae. The primary Laves phase grew to several tens of micrometers and the eutectic Laves lamellae are distributed in the interdendritic B2 phase (Fig. 1d). The lamella thicknesses of eutectic Laves phase range from several hundred nanometers to several micrometers. A high magnification image of dual-phase lamellar structure of Nb20 alloy is shown in Fig. 4a. The different regions with bright and dark contrasts are the B2 and Laves phases, respectively. This is because the B2 phase was thinner than the Laves phase, resulting from the different milling rate during ion milling. Fig. 4b and c show the TEM-SAED (selected-area electron diffraction) patterns of B2 and hexagonal Laves phases with zone axes of [0 0 1] and [2–1–10], respectively. The presence of superlattice spots obtained from B2 phase (marked by red circle in Fig. 4b) reveals the ordered BCC structure of NiAl-rich phase. From the phase distributions in Fig. 3d-f, the volume fraction of FeNb-rich Laves phase increased from 9.7% (Nb5 alloy) to 28.3% (Nb10 alloy), then to 61.8% (Nb20 alloy). The Laves phases of both Nb5 and Nb10 alloys are distributed in the interdendritic regions. In addition, the Laves phases in Nb10 alloy have various crystal orientation, confirmed by the variational color (Fig. 3b). This result is consistent with the XRD pattern of Nb10 alloy (Fig. 2).

The measured microhardness of three as-cast HEAs are plotted in Fig. 4d. Nb5 alloy has an average hardness of 505.2 HV, which is close to the HPT-processed single-phase FCC CoCrFeMnNi HEA [7]. This is attributed to the dominating B2 phase with high hardness in Nb5 alloy. With the increase of Nb content, the hardness dramatically increased due to the incremental volume fraction of Laves phase. Eventually, the

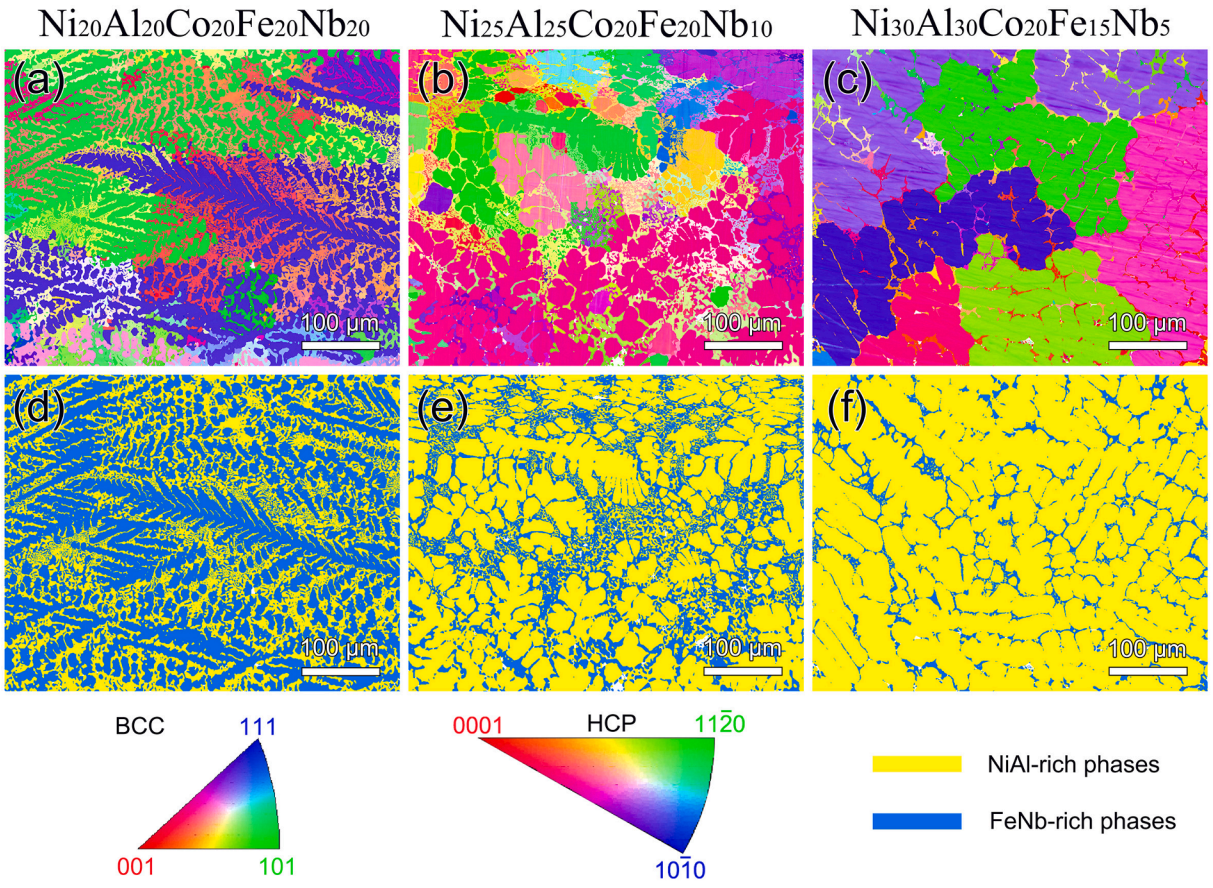

Fig. 3. Crystal orientation (a-c) and phase distribution (d-f) of (a, d) Nb20, (b, e) Nb10 and (c, f) Nb5 HEAs.

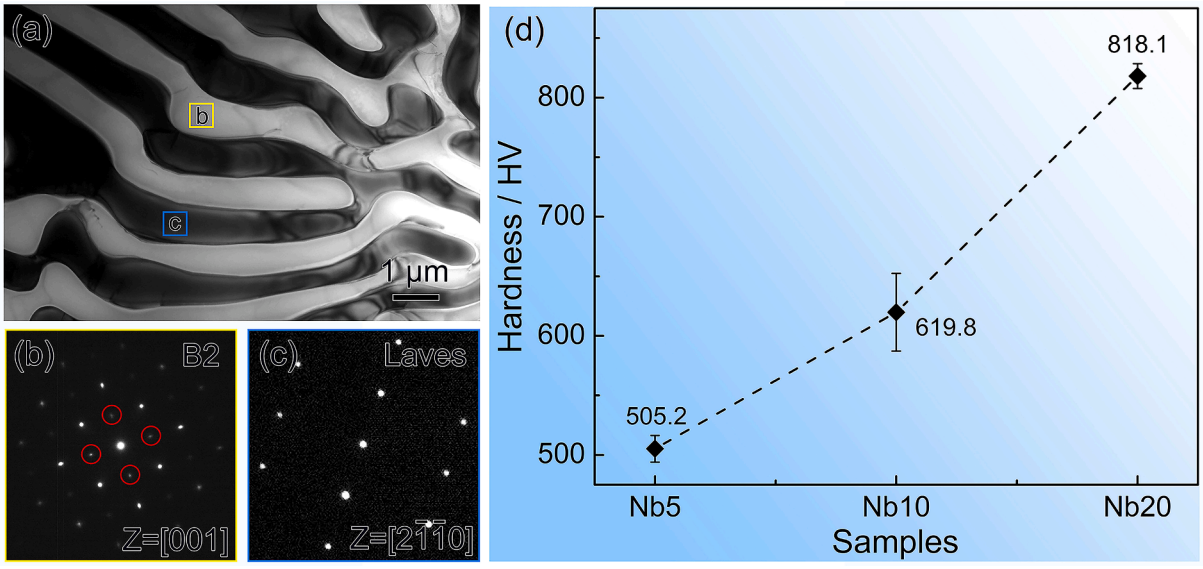

Fig. 4. (a) Bright-field TEM image of $Ni_{20}Al_{20}Co_{20}Fe_{20}Nb_{20}$ HEA with lamellar structure. The SAEDs corresponding to (b) B2 (NiAl-rich) and (c) Laves (FeNb-rich) phases, respectively. (d) Microhardness evolution as the increase of Nb content.

average hardness increased to an ultrahigh value of 818.1 HV for the equiatomic Nb20 alloy. The hardness of Laves phase is about 1059.2 HV, which exceeds twice as hard as B2 phase (483.7 HV). On the basis of the rule of mixture, the calculated hardness of Nb5, Nb10 and Nb20 alloys are 539.5, 646.5 and 839.3 HV, respectively, close to the actual measured average hardness values.

4. Conclusions

In this work, three dual-phase HEAs containing equiatomic or non-equiatomic NiAlCoFeNb were prepared by vacuum arc melting. The microstructure, phase constitution and microhardness of all three as-cast HEAs were investigated. These HEAs were all composed of NiAl-rich B2

phase and FeNb-rich hexagonal Laves phase. It was verified that the average hardness dramatically increased from 505.2 HV of $Ni_{30}Al_{30}Co_{20}Fe_{15}Nb_5$ alloy to 818.1 HV of $Ni_{20}Al_{20}Co_{20}Fe_{20}Nb_{20}$ alloy with the increased volume fraction of Laves phase from 9.7% to 61.8%. The FeNb-rich Laves phase can be applied to strengthening the other HEAs system.

CRediT authorship contribution statement

Lei Gu: Conceptualization, Data curation, Visualization, Investigation, Methodology, Writing – original draft. **Ningning Liang:** Supervision, Funding acquisition, Writing – review & editing. **Yi Liu:** Investigation, Methodology, Writing – review & editing. **Yuyao Chen:** Investigation, Methodology. **Jihua Liu:** Investigation. **Yixing Sun:** Investigation. **Yonghao Zhao:** Methodology, Supervision, Validation, Funding acquisition.

Declaration of Competing Interest

The authors declare that they have no known competing financial interests or personal relationships that could have appeared to influence the work reported in this paper.

Acknowledgements

This work was supported by the National Key R&D Program of China (Grant No. 2021YFA1200203, 2017YFA0204403), National Natural Science Foundation of China (Grant No. 51971112, 51225102, 52105368), Fundamental Research Funds for the Central Universities (Grant No. 30919011405) and Natural Science Foundation of Jiangsu Province, China (Grant No. BK20190478). Lei Gu acknowledges the support by Large-scale Instrument and Equipment Open Fund of Nanjing University of Science and Technology.

References

[1] J.W. Yeh, S.K. Chen, S.J. Lin, et al., Adv. Eng. Mater. 6 (2004) 299–303.
[2] B. Cantor, I.T.H. Chang, P. Knight, et al., Mater. Sci. Eng. A 375–377 (2004) 213–218.
[3] W. Jiang, X. Gao, Y. Cao, et al., Mater. Sci. Eng. A 837 (2022), 142735.
[4] D. Kong, W. Wang, T. Zhang, et al., Mater. Lett. 311 (2022), 131613.
[5] Y. Cao, S. Ni, X.Z. Liao, et al., Mater. Sci. Eng. R: Rep. 133 (2018) 1–59.
[6] Q. Mao, Y. Liu, Y. Zhao, J. Alloy. Compd. 896 (2022), 163122.
[7] B. Schuh, F. Mendez-Martin, B. Völker, et al., Acta Mater. 96 (2015) 258–268.
[8] F. Wei, S. Wei, K.B. Lau, et al., Materialia 21 (2022), 101308.
[9] F. He, Z. Wang, P. Cheng, et al., J. Alloy. Compd. 656 (2016) 284–289.
[10] J. Tuo, R. Zhang, Z. Cai, et al., J. Nucl. Mater. 561 (2022), 153561.
[11] A.A.A.P. Silva, M.S. Lamoglia, G. Silva, et al., J. Alloy. Compd. 878 (2021), 160411.